

Preparation of Strongly Correlated Superconducting States on a Quantum Computer with Hints of Quantum Advantage

LeeAnn M. Sager and David A. Mazziotti*

Department of Chemistry and The James Franck Institute, The University of Chicago, Chicago, IL 60637

(Dated: Submitted January 20, 2021)

One of the most correlated quantum phenomena achievable is superconductivity. In superconductivity pairs of electrons condense, in a manner analogous to Bose-Einstein condensation, into the same quantum state with their subsequent entanglement permitting frictionless conductivity. Quantum computers have the potential to predict complex, entangled quantum states at non-exponential cost, unlike their classical counterparts, with possible applications to hard problems from physics to economics. Here, using pairs of qubits to represent the electron pairs, we create superconductivity on a transmon-qubit quantum computer. A series of maximally entangled superconducting states with different numbers of electron pairs is prepared, and then the occupation of the superconducting state is measured by tomography. Each occupation on the order of the number of electrons $O(N)$ confirms the formation of a maximally entangled superconducting state. Moreover, the large eigenvalue provides experimental validation of C. N. Yang's derivation of large occupation being associated with off-diagonal long-range order. The work provides a critically important step in predicting strongly entangled quantum physics as well as mathematically related non-local phenomena in the pure and social sciences on quantum computers.

Significant theoretical and experimental investigation has centered on strongly correlated materials—especially superconductivity [1–9]—over the previous century [10–14]. Recently, quantum computers have emerged as potentially powerful calculators of strongly correlated systems [15–23] as high-entanglement states can be programmatically generated at non-exponential cost, foreshadowing the emergence of a significant advantage of quantum computers over classical computers for certain classes of problems—a phenomenon known as quantum advantage [24, 25]. Here, we prepare superconductivity on a quantum computer by entangling pairs of qubits into Cooper-like bosonic pairs (see Fig. 1) to form extreme superconducting states whose quantum tomography directly measures the off-diagonal long-range order [12, 26–32], first predicted by C. N. Yang in 1962. Consequently, we prepare a gold-standard correlated state that depends upon an exponentially-scaling number of orbital-product configurations, thereby harnessing the beginnings of quantum advantage (see Fig. 2). Further, such programmable superconducting states may prove useful for analyzing, benchmarking, and probing properties of superconductors with potential applications in spintronics, magnetic materials, and renewable energy.

Results:

The Superconducting Wavefunction and Quantum State Preparation. Our superconducting state on the quantum computer was prepared by entangling pairs of qubits into Cooper-like bosonic states such that the two-body wavefunction of each pair (i.e., the geminal) is given by

$$\frac{1}{\sqrt{2}} [|00\rangle_{i,j} + |11\rangle_{i,j}] \quad (1)$$

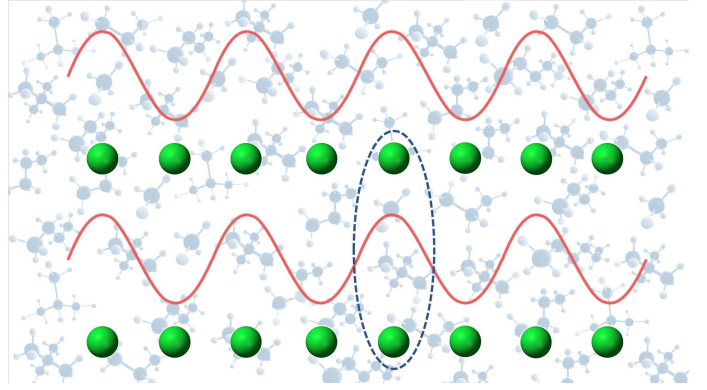


FIG. 1: A schematic demonstrating the interpretation of the Cooper pairing of electrons to create an overall bosonic state in a quantum system.

where i and j are indices that represent orbitals that correspond to specific qubits and where $|00\rangle$ and $|11\rangle$ represent doubly unfilled and doubly filled orbitals corresponding to those specified orbitals.

For an r -qubit system, the overall prepared quantum state was then constructed via tensor multiplication of $r/2$ distinct geminals

$$|\Psi\rangle = \bigotimes_{p=0}^{r/2-1} \frac{1}{\sqrt{2}} [|00\rangle_{2p,2p+1} + |11\rangle_{2p,2p+1}] \quad (2)$$

where p specifies the pair index and adjacent qubits with qubit indices $2p$ and $2p+1$ are paired by definition. (See the Methods section for the gate sequence utilized to obtain this quantum state.) The above preparation yields an entangled state composed of substates with all possible, paired, even-numbered excitations—with the overall entangled state able to be separated into number-

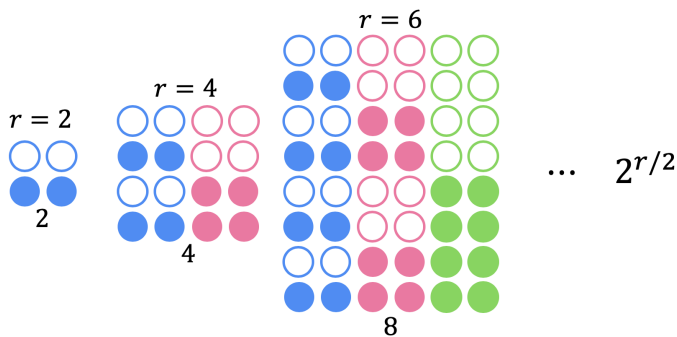


FIG. 2: A schematic demonstrating the possible configurations (i.e., each row) for a given number r of qubits where a filled circle indicates the $|1\rangle$ state which corresponds to an occupied orbital and an unfilled circle represents the $|0\rangle$ state which corresponds to an unoccupied orbital.

conserving substates with even particle numbers—i.e., substates of zero, two, four, ..., $r - 2$, and r particles for an r -qubit system—via post-measurement analysis (see Sec. IIA of the Supplemental Information).

Importantly, as the overall, resultant wavefunction is a tensor product of geminals, the size of the entangled wavefunction scales exponentially with system size, which would present exponential costs for classical computation. Even though the number of orbital-product configurations contributing to the wavefunction scales exponentially, the special tensor product structure of this wavefunction can be exploited to obtain a two-particle reduced density matrix (2-RDM) of this state that can be computed on a classical computer at polynomial cost [30]. However, as can be seen from the algorithm for the preparation of the overall quantum state (see the Methods section), this wavefunction can be prepared directly on quantum devices through the application of quantum gates without such exponential scaling, which offers hints of quantum advantage to probing such a highly correlated quantum state on a quantum device. Furthermore, modifying the wavefunction may provide a route to more-complicated strongly correlated quantum states that can be prepared on a quantum computer at polynomial cost despite the absence of non-exponentially-scaling representations of these states on the classical computer.

As an example, this procedure yields a wavefunction given by

$$|\Psi\rangle = \frac{1}{2}[|0000\rangle + |1100\rangle + |0011\rangle + |1111\rangle] \quad (3)$$

for a system of $r = 4$ qubits. Note that the overall $r = 4$ wavefunction is an entangled state constructed of three number-conserving substates given by

$$|\Psi_0\rangle = |0000\rangle, \quad (4)$$

$$|\Psi_2\rangle = \frac{1}{\sqrt{2}}[|1100\rangle + |0011\rangle], \quad (5)$$

and

$$|\Psi_4\rangle = |1111\rangle \quad (6)$$

with $N = 0, 2$, and 4 particles, respectively. These substates can be probed directly by probing the entangled state and projecting out a specified particle number (see the Supplemental Information.)

Measuring the Signature of Superconductivity. In order to measure whether the experimentally-prepared quantum state and/or the number-conserving substates projected out from the overall ensemble state demonstrate superconductivity, we conduct quantum tomography (see the Supplemental Information for details) to probe directly the presence and extent of off-diagonal long-range order, which is a computational signature of superconductivity. To determine the presence and degree of this long-range order for a specified quantum state, it is useful to establish a calculable, characteristic property [12, 26–32]. Such a signature of superconductivity is a large eigenvalue in the particle-particle reduced density matrix (RDM) [27, 28], with elements given by

$${}^2D_{k,l}^{i,j} = \langle \Psi | \hat{a}_i^\dagger \hat{a}_j^\dagger \hat{a}_k \hat{a}_l | \Psi \rangle \quad (7)$$

where $|\Psi\rangle$ is an N -fermion wavefunction, each index (i, j, k, l) represents a one-fermion spin orbital in a finite basis set with rank r , and \hat{a}^\dagger and \hat{a} are fermionic creation and annihilation operators respectively. We define the largest eigenvalue of the particle-particle RDM to be λ_D , and as this value indicates the degree of off-diagonal long-range order [27, 28], it is a signature of the presence and extent of superconductivity, with values above one signifying a superconducting quantum state.

Analysis on the presence and extent of superconductivity (measured via λ_D) of both the overall entangled state ($|\Psi\rangle$) and the number-conserving substates is conducted for various numbers r of total qubits in the following sections.

Superconductivity Before Imposition of Particle Number Conservation. The overall entangled state was prepared for both simulation and an experimental quantum device for all even-numbered qubit systems from $r = 0$ to $r = 14$. Post-measurement computation of the quantum signature of superconductivity (λ_D) was then employed to probe the presence and extent of superconductivity for these overall states. As can be seen in Figure 3, the signature of superconductivity increases as the number r of qubits comprising the system is increased, and—for simulation—superconductivity is observed (i.e., $\lambda_D > 1$) for all prepared states with $r \geq 8$. While the experimental results deviate from simulation due to the noisy nature of near-term quantum devices [33] (see Methods for device specifications and the Supplemental Information for errors), experimental systems

with $r = 12$ and $r = 14$ qubits did demonstrate superconductivity. Further, the trend of the extent of superconductivity increasing as the number of qubits comprising the system increases holds for the experimental results, which is promising for future efforts to probe more macroscopically-scaled superconducting materials on quantum devices.

As can be seen from Eqs (4) and (6), the overall entangled states have components that obviously do not contribute to superconductivity as these components are not entangled; thus, the other substates must have a larger degree of superconductivity than the overall ensemble state. Additionally, real-world superconducting materials should conserve particle number. It is hence beneficial to probe the number-conserving substates that comprise the overall entangled state in order to both isolate the superconducting behavior of the number-conserving substates and to more-closely model real-world superconductivity.

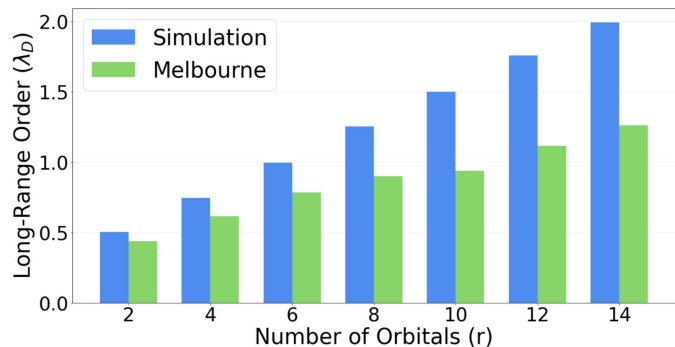


FIG. 3: The λ_D values for the overall ensemble state preparation for simulation and experimental melbourne results.

Superconductivity in Number-Conserving Substates.

By projecting out a specific number of particles from the results obtained for overall entangled state (see the Supplemental Information), we can probe the behavior and properties of the number-conserving substates. Specifically, as is shown in Fig. 4, the extent of superconductivity (λ_D) for each number-conserving state can be isolated from the overall r -qubit preparation described in Eq. (2). As can be seen from the simulation results, all number-conserving substates with $2 < N < r$ demonstrate superconductivity ($\lambda_D > 1$) where $N = 2$ fails to demonstrate condensation behavior as the maximum signature of condensation is $N/2$ for even N -particle systems [27, 28] and as $N = r$ fails to demonstrate condensation behavior as this substate ($|1\rangle^{\otimes r}$) is not entangled. Further, the signature of condensation seems to follow a bell curve centered around $(r + 2)/2$ such that maximum superconductivity is observed at half fill-

ing for $N = (r + 2)/2$ if $(r + 2)/2$ is even and for both $N = (r + 2)/2 - 1$ and $(r + 2)/2 + 1$ if $(r + 2)/2$ is odd. Again, the extent of superconductivity is lesser for the experimental results for all particle-conserving states due to experimental error; however, the qualitative trends described for simulation hold in general although the bell curve does demonstrate a slight negative (right-modal) skew, implying that the quantum computer does not exactly treat the particle and hole statistics symmetrically. Importantly, superconductivity is clearly observed for $r = 14$ experimental results for particle numbers $N \geq 6$. Note that although only results for the largest-qubit preparation ($r = 14$) are shown, all data is included in the Supplemental Information; the trends in the $r = 14$ data hold for the lower-qubit results, and additionally, the $r = 14$ qubit data demonstrates the largest signature of superconductivity as the largest eigenvalue λ_D value for a fixed N increases as the number r of qubits is increased.

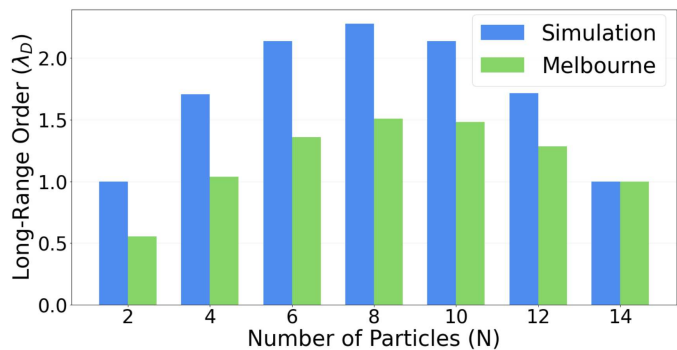


FIG. 4: The λ_D values for the number-conserving substates of rank $r = 14$ for simulation and experimental melbourne results.

Discussion and Conclusions:

In this study we use a transmon quantum computer—where each qubit is composed of a microwave phonon in an anharmonic well potential—as a programmable “material” on which we have prepared and probed superconducting states, which represent a prototypical highly entangled form of matter with well-established potential applications in energy transport and electronics [1–6]. This is done by constructing r -qubit quantum states by entangling $r/2$ disjunct pairs of adjacent qubits to create overall states composed of individual particle-conserving double, quadruple, \dots , and r -tuple paired excitations. This highly entangled state scales exponentially with the rank r of the system (see Fig. 2). The inherent parallelism of quantum computers, however, allows such states to be prepared and probed in a much more facile manner, thereby providing important hints of quantum advantage [24, 25].

The overall entangled state is shown to demonstrate increasing character of superconductivity as the number r of qubits is increased through use of post-measurement computation of the signature of superconductivity [27, 28] for experiments conducted on both a qasm simulator and an IBM quantum experience device. Further, we analyze the extent of superconductivity for the individual particle-conserving components of the overall quantum states by projecting out specified particle-number information from the data obtained for the overall wavefunction. From this, we observe that for a given number of qubits (r), the signature of superconductivity—a large eigenvalue in the particle-particle RDM—follows the expected bell curve [30]. This increasing superconducting character as the size of the material (i.e., the number of qubits) is increased is promising for the development of more macroscopically-scaled, programmable superconducting materials as the size of quantum devices in the future continues to increase.

This study advances both the fields of quantum computation and superconductivity as we have prepared a strongly correlated “material” on a quantum device, which provides a facile, reproducible, and cloud-accessible manner for the creation of a novel superconducting state. Further, as the number of gates employed for the preparation of the strongly correlated quantum state scales linearly with r —as opposed to the exponential scaling of classical simulations—,this study demonstrates the beginnings of a quantum advantage over classical simulation for applications in highly entangled materials. Construction of such so-called superconducting material at linear costs may be ideal for testing, benchmarking, and analyzing superconducting states in future applications. In any manner, this study represents the first step in the creation and analysis of a programmable superconducting “material” on a quantum device.

Methods:

We include details on the quantum algorithm used to prepare the qubit states presented in the article; explain the inherent bosonification of the state preparation employed throughout this text; briefly describe the errors inherent to near-term quantum computers; and provide relevant details on the experimental quantum device employed.

Quantum algorithm for state preparation. The overall quantum state is composed of all pairwise even excitations of the $r/2$ individually-paired qubits. This preparation is accomplished by

$$|\Psi\rangle = \left[\prod_{p=0}^{r/2-1} C_{2p}^{2p+1} H_{2p} \right] |0\rangle^{\otimes r} \quad (8)$$

where $|0\rangle^{\otimes r}$ is the initial quantum state in which all qubits are in their ground state, p represents the index of each of the possible $r/2$ adjacent, paired qubits, H_i is the Hadamard gate acting on Q_i , and C_i^j is a CNOT gate

with Q_i and Q_j acting as the control and target qubits, respectively. Application of the gate sequence given in Eq. (8) produces the wavefunction described by Eq. (2).

Inherent bosonification in the state preparation. In general, when probing fermionic statistics on a quantum device, some transformation—such as the Jordan-Wigner transformation—must be built into both state preparation and analysis in order to account for the anticommutation relationships that fermions must satisfy. However, in our preparation described in Eq (2), pairs of fermions are deliberately constructed creating inherently bosonic geminal states. The antisymmetrization is hence buried into the bozonized pairs and allows for a compact mapping to generate and probe the quantum states created.

Description of noise on near-term quantum devices. Three main classes of errors lead to the deviation of physical qubits from the idealized logical qubits: namely, gate noise, readout noise, and decoherence. Quantum gate noise/error refers to a situation where the application of a unitary gate \hat{U} to a quantum state $|\Psi\rangle$ yields a result that deviates from $\hat{U}|\Psi\rangle$. This class of error is caused by either imprecisely calibrated control of the qubits and/or imperfect isolation of qubits from their environment, and the overall gate error increases with the number of gates applied. Readout noise/error refers to transmission line noise that makes the $|0\rangle$ state appear to be $|1\rangle$ or vice versa; it can be caused by the probability distributions of the measured physical quantities that correspond to the $|0\rangle$ and $|1\rangle$ states overlapping and/or the qubit decaying during readout. Decoherence involves interactions with external systems (vibrations, temperature fluctuations, electromagnetic waves, etc.) leading to the degradation of the quantum state prepared on quantum devices. As both the number of gates applied to a system—and hence gate noise—and decoherence tend to increase with system size (r), larger-scale quantum computations often involve more and more error [33]. See the Supplemental Information of Ref. 23 for a more thorough exploration of error on near-term quantum devices.

Experimental quantum device specifications. Throughout this work, we have employed the `ibmqx_16_melbourne` [34] IBM Quantum Experience device, which is available online. This Quantum device is composed of fixed-frequency transmon qubits with coplanar waveguide resonators [35, 36]. Experimental calibration data and connectivity for this device is included in Supplemental Information.

Data availability. Data will be made available upon reasonable request.

Code availability. Code will be made available on a public Github repository upon publication.

Acknowledgments: D.A.M. gratefully acknowledges the Department of Energy, Office of Basic Energy Sciences, Grant DE-SC0019215 and the U.S. National Science Foundation Grants No. CHE-2035876, No. DMR-

2037783, and No. CHE-1565638.

* damazz@uchicago.edu

- [1] J. Bardeen, L. N. Cooper, and J. R. Schrieffer, "Theory of superconductivity," *Phys. Rev.* **108**, 1175–1204 (1957).
- [2] J. M. Blatt, "Electron pairs in the theory of superconductivity," *Progress of Theoretical Physics* **23**, 447–450 (1960).
- [3] Philip W Anderson, "Twenty-five years of high-temperature superconductivity – a personal review," *Journal of Physics: Conference Series* **449**, 012001 (2013).
- [4] A. P. Drozdov, P. P. Kong, V. S. Minkov, S. P. Besedin, M. A. Kuzovnikov, S. Mozaffari, L. Balicas, F. F. Balakirev, D. E. Graf, V. B. Prakapenka, E. Greenberg, D. A. Knyazev, M. Tkacz, and M. I. Eremets, "Superconductivity at 250 k in lanthanum hydride under high pressures," *Nature* **569**, 528–31 (2019).
- [5] V L Ginzburg, "High-temperature superconductivity (history and general review)," *Soviet Physics Uspekhi* **34**, 283–288 (1991).
- [6] A Glatz, I A Sadovskyy, U Welp, W-K Kwok, and G W Crabtree, "The quest for high critical current in applied high-temperature superconductors," *J. Supercond. Nov. Magn.* **33**, 127–141 (2020).
- [7] Y. Cao, V. Fatemi, S. Fang, K. Watanabe, T. Taniguchi, E. Kaxiras, and P. Jarillo-Herrero, "Unconventional superconductivity in magic-angle graphene superlattices," *Nature* **556**, 43–50 (2018).
- [8] Y. Cao, D. Rodan-Legrain, O. Rubies-Bigorda, J. Min Park, K. Watanabe, T. Taniguchi, and P. Jarillo-Herrero, "Tunable correlated states and spin-polarized phases in twisted bilayer-bilayer graphene," *Nature* **583**, 215–220 (2020).
- [9] A. Uri, S. Grover, Y. Cao, J. Crosse, K. Bagani, D. Rodan-Legrain, Y. Myasoedov, K. Watanabe, T. Taniguchi, P. Moon, and et al., "Mapping the twist-angle disorder and landau levels in magic-angle graphene," *Nature* **581**, 47–52 (2020).
- [10] E. Tutuc, M. Shayegan, and D. A. Huse, "Counterflow measurements in strongly correlated GaAs hole bilayers: evidence for electron-hole pairing," *Phys. Rev. Lett.* **93**, 36802 (2004).
- [11] D. V. Fil and S. I. Shevchenko, "Electron-hole superconductivity (review)," *Low Temp. Phys.* **44**, 867–909 (2018).
- [12] S. Safaei and D. A. Mazziotti, "Quantum signature of exciton condensation," *Phys. Rev. B* **98**, 045122 (2018).
- [13] A. Kogar, M. S. Rak, S. Vig, A. A. Husain, F. Flicker, Y. I. Joe, L. Venema, G. J. MacDougall, T. C. Chiang, E. Fradkin, J. van Wezel, and P. Abbamonte, "Signatures of exciton condensation in a transition metal dichalcogenide," *Science* **358**, 1314–1317 (2017).
- [14] X. Liu, K. Watanabe, T. Taniguchi, B. I. Halperin, and P. Kim, "Quantum Hall drag of exciton condensate in graphene," *Nat. Phys.* **13**, 746–750 (2017).
- [15] F. Verstraete, J. I. Cirac, and J. I. Latorre, "Quantum circuits for strongly correlated quantum systems," *Phys. Rev. A* **79** (2009).
- [16] P. Smith-Goodson, "Quantum volume: A yardstick to measure the performance of ..." (2019).
- [17] G. J. Mooney, C. D. Hill, and L. C. L. Hollenberg, "Entanglement in a 20-qubit superconducting quantum computer," *Scientific Reports* **9** (2019).
- [18] R. Ma, B. Saxberg, C. Owens, N. Leung, Y. Lu, J. Simon, and D. I. Schuster, "A dissipatively stabilized Mott insulator of photons," *Nature* **566**, 51–57 (2019).
- [19] H.-L. Huang, D. Wu, D. Fan, and X. Zhu, "Superconducting quantum computing: a review," *Science China Information Sciences* **63** (2020).
- [20] S. Mcardle, S. Endo, A. Aspuru-Guzik, S. C. Benjamin, and X. Yuan, "Quantum computational chemistry," *Rev. Mod. Phys.* **92** (2020).
- [21] K. Head-Marsden, J. Flick, C. J. Ciccarino, and P. Narang, "Quantum information and algorithms for correlated quantum matter," *Chem. Rev.* (2021), [10.1021/acs.chemrev.0c00620](https://doi.org/10.1021/acs.chemrev.0c00620).
- [22] S. E. Smart and D. A. Mazziotti, "Quantum-classical hybrid algorithm using an error-mitigating n-representability condition to compute the mott metal-insulator transition," *Phys. Rev. A* **100** (2019), [10.1103/physreva.100.022517](https://doi.org/10.1103/physreva.100.022517).
- [23] L. M. Sager, S. E. Smart, and D. A. Mazziotti, "Preparation of an exciton condensate of photons on a 53-qubit quantum computer," *Phys. Rev. Research* **2**, 043205 (2020).
- [24] F. Arute, K. Arya, R. Babbush, D. Bacon, J. C. Bardin, R. Barends, R. Biswas, S. Boixo, F. G. S. L. Brandao, D. A. Buell, and et al., "Quantum supremacy using a programmable superconducting processor," *Nature* **574**, 505–510 (2019).
- [25] V. E. Elfving, B. W. Broer, M. Webber, J. Gavartin, M. D. Halls, K. P. Lorton, and A. D. Bochevarov, "How will quantum computers provide an industrially relevant computational advantage in quantum chemistry?" *arXiv*, 1–20 (2020).
- [26] Oliver Penrose and Lars Onsager, "Bose-einstein condensation and liquid helium," *Phys. Rev.* **104**, 576–584 (1956).
- [27] C. N. Yang, "Concept of off-diagonal long-range order and the quantum phases of liquid He and of superconductors," *Rev. Mod. Phys.* **34**, 694–704 (1962).
- [28] F. Sasaki, "Eigenvalues of fermion density matrices," *Phys. Rev.* **138**, B1338–B1342 (1965).
- [29] A. J. Coleman, "Structure of fermion density matrices," *Rev. Mod. Phys.* **35**, 668–686 (1963).
- [30] A. J. Coleman, "Structure of fermion density matrices. ii. antisymmetrized geminal powers," *J. Math. Phys.* **6**, 1425–31 (1963).
- [31] L. M. Sager, S. Safaei, and D. A. Mazziotti, "Potential coexistence of exciton and fermion-pair condensations," *Physical Review B* **101**, 081107 (2020).
- [32] A. Raeber and D. A. Mazziotti, "Large eigenvalue of the cumulant part of the two-electron reduced density matrix as a measure of off-diagonal long-range order," *Physical Review A* **92**, 052502 (2015).
- [33] J. Preskill, "Quantum computing in the nisq era and beyond," *Quantum* **2**, 79 (2018).
- [34] IBM-Q-Team, "IBM-Q-15 Melbourne backend specification v2.0.0," (2019).
- [35] J. Koch, T. M. Yu, J. Gambetta, A. A. Houck, D. I. Schuster, J. Majer, A. Blais, M. H. Devoret, S. M. Girvin, R. J. Schoelkopf, and et al., "Charge-insensitive qubit design derived from the cooper pair

- box,” [Physical Review A](#) **76** (2007).
- [36] J. M. Chow, A. D. Córcoles, J. M. Gambetta, C. Rigetti, B. R. Johnson, J. A. Smolin, J. R. Rozen, G. A. Keefe, M. B. Rothwell, M. B. Ketchen, and et al., “Simple all-microwave entangling gate for fixed-frequency superconducting qubits,” [Physical Review Letters](#) **107** (2011).